Agricultural Water Management 258 (2021) 107204

Contents lists available at ScienceDirect

Agricultural Water Management

journal homepage: www.elsevier.com/locate/agwat

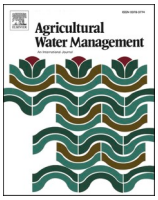

Satellite rainfall bias assessment for crop growth simulation – A case study of maize growth in Kenya

Calisto Kennedy Omondi [a,*], Tom H.M. Rientjes [a], Martijn J. Booij [b], Andrew D. Nelson [a]

[a] Faculty of Geo-information Science and Earth Observation (ITC), University of Twente, Enschede 7500 AE, The Netherlands
[b] Department of Water Engineering and Management, Faculty of Engineering Technology, University of Twente, Enschede 7500 AE, The Netherlands

ARTICLE INFO

Handling editor Xiying Zhang

Keywords:
Bias
Crop growth simulation
Crop growth stages
Lake Victoria basin
Remote sensing
Satellite-based rainfall

ABSTRACT

In this research, the performance of satellite rainfall estimates (SREs) for crop growth simulation was investigated. Rainfall products selected were CHIRPS 2.0, CMORPH 1.0, MSWEP 2.2, and RFE 2.0. In-situ rainfall from 20 stations within the Lake Victoria basin in Kenya served as reference. Rainfall products were evaluated for onset days, rainfall depths, dry spells, and rainfall occurrence for four crop growth stages. Assessment was on a daily time step for the period 2012–2018 and on a point-to-pixel basis. Results showed that SREs exhibit large variation in timing of rainfall arrival. SREs exhibited largest interannual and spatial spreads in representing dry spell length during the flowering stage with CMORPH and CHIRPS showing best and weakest results, respectively. Bias of SREs in representing dry spells was smaller during early growth stages. Detecting rainfall occurrence by the SREs weakened as the growing season progressed. MSWEP, followed by RFE2, produced the best results in detecting rainfall events, while falsely detected rainfall was frequent in CHIRPS, particularly in later growth stages. SREs generally performed better during a wet than a dry growing season. SREs indicated less bias in rainfall depths during the early stages of crop growth but deteriorated at later stages. MSWEP and CMORPH exhibited the least and highest interannual spread in relative bias, respectively. In associating biases to severe and extreme water stress, based on crop water requirement satisfaction index, effects were more prevailing in the ripening than flowering stages. Findings of this study suggest that SREs can serve as input to crop growth modelling, but validation of SREs with rain gauge observed counterparts is essential.

1. Introduction

Crop growth simulation approaches commonly are used to assess the impact of environmental factors, management practices, and plant genetics on crop development at plot or field scales (Thaler et al., 2018). Simulation approaches differ in complexity and input data requirements subject to intended use. Physically-based crop growth models, which incorporate mathematical descriptions of the main crop growth processes, provide quantitative descriptions of the mechanisms that cause crop growth and development (Hoogenboom, 1991). Such approaches simulate crop growth (e.g., biomass partitioning, water use) and development (e.g., phenology) across various cropping stages, normally from seeding until physiological maturity. Despite noticeable development on crop growth simulations since the mid-1960s (Duncan et al., 1967), the limited availability and quality of input data remain challenging, causing uncertainty in simulated outputs. Representation of crop growth processes in simulations requires an understanding of the role of (i) *driving variables* (e.g., meteorological data); (ii) *state variables* (e.g., number of leaves) that characterize the state of a crop growth system; (iii) *model parameters* to parameterize relationships between driving and state variables (e.g., soil characteristic data); and (iv) *output variables* (Thaler et al., 2018).

Among various variables influencing simulated crop growth characteristics, soil moisture has been identified as one of the most important variables (Riha et al., 1996; Watson and Challinor, 2013). Ban et al. (2019) showed that soil moisture shortage is the most crucial crop growth-limiting factor. Shortage of soil moisture causes reduction of growth and is commonly referred to as crop water stress. Effective rainfall, the difference between rainwater and actual evapotranspiration (AET) that is retained in the rootzone for meeting crop water requirement (WR) (Ali and Mubarak, 2017), is the primary source of soil moisture under rainfed agriculture and, thus, the most critical meteorological input variable in crop growth analyses.

Crop growth in relation to rainfall and water stress has been studied

* Corresponding author.
E-mail address: c.k.omondi@utwente.nl (C.K. Omondi).

https://doi.org/10.1016/j.agwat.2021.107204
Received 27 May 2021; Received in revised form 13 September 2021; Accepted 21 September 2021
Available online 7 October 2021

considering multiple rainfall characteristics, as summarized in Table 1. Studies indicate that crop growth responses to rainfall vary for different crops subject to the crop growth stage and growth requirements for water.

Most relevant rainfall characteristics that directly affect crop growth are rainfall onset to denote the start of the cropping season, dry spell indicating periods without rainfall, duration of rainy periods and rainfall intensity to indicate how much it rains, and occurrence to indicate the frequency of rain events. *Rainfall onset* (Tadross et al., 2007) and antecedent rainfall conditions affect soil moisture conditions and, thus, define the seeding time for rainfed agriculture (Yadav et al., 2013). Both rainfall arrival and antecedent soil moisture conditions are critical inter-seasonal rainfall representations for crop emergence and establishment in crop growth simulations. Wrongly identified rainfall arrival by SREs may result in incorrect timing of seeding in simulation applications and may cause uncertain simulated outputs. Misrepresenting *dry spell* length directly influences soil moisture storage from rainfall for all growth stages with propagation effects on crop simulation results. Under- or over-estimating *rainfall depths* could result in soil moisture shortages or cause waterlogging for crops, respectively. *Prolonged rainfall intervals* and soil moisture shortages from pre-flowering to grain filling can lead to late maturity or loss of grain production, respectively. In reality, high rainfall can result in rotting or fungal infections affecting the ripening phase. During the vegetative and flowering stages, severe water stress affects leaf area development due to a decrease in the stomatal opening, which limits CO_2 uptake leading to a reduced rate of photosynthesis (Osakabe et al., 2014).

Crop growth simulations require rainfall characteristics to be well represented with accurate estimates so to make simulation results useful. *Accuracy* is the closeness of agreement between a measured and true value of the quantity being measured (Joint Committee For Guides In Metrology, 2012). However, representing real world rainfall distributions and characteristics is challenging in crop growth simulations. Errors in rainfall representation propagate to simulated outputs (McMillan et al., 2011). Misrepresentation of rainfall characteristics cause uncertainty and possibly errors in simulated results through error propagation. In this respect, Guo et al. (2015) showed that errors in simulated soil moisture deficit can lead to decreased leaf water potential causing reduced leaf growth besides increasing dry matter allocation to the roots, decreased root-to-shoot ratio, and reduced biomass or retarded growth of non-drought tolerant crops. Sah et al. (2020) showed that soil moisture stress increases days to flowering, days to maturity, anthesis silk interval, decreases total leaf number, and loss of normal root architecture leading to reduced biomass. Errors in simulated soil saturation by excessive rainfall can lead to O_2 restrictive conditions affecting plant growth, development and survival (Parent et al., 2008). Comparing differences in growth and physiological performance of plants under soil waterlogging stress, Yang et al. (2020) showed reduced photosynthesis during waterlogging that soon recovered on draining.

Table 1
Key rainfall characteristics affecting crop growth.

Rainfall characteristic/ index	Studies /description
Onset day	The onset of the rains (Bombardi et al., 2017; Ndamani and Watanabe, 2015; Sultan et al., 2019)
Rainfall depth	Aggregated rainfall depth for period considered (Guan et al., 2015; Luetkemeier et al., 2018; Sultan et al., 2019)
Rainy days	Number of days within a specified period with a rainfall event above 1 mm (Guan et al., 2015; Ndamani and Watanabe, 2015; Sultan et al., 2019)
Rainfall events	Number of days within a specified period with rainfall exceeding certain thresholds [mm day^{-1}] (Sultan et al., 2019)
Rainfall intensity	The ratio between rainfall depth and rainy days within a specified period (Guan et al., 2015; Li et al., 2019; Sultan et al., 2019)
Dry spell	Number of consecutive days between two rainfall events above 1 mm (Fall et al., 2021; Guan et al., 2015)
Cessation day	The demise of rains (Bombardi et al., 2017; Sivakumar, 1988)
Soil water stress factor	The ratio between AET and potential evapotranspiration used in calculating daily leaf area and yield increments. In assimilating remote sensing data in a crop growth assessment, Ban et al. (2019) estimated soil water stress factors using daily crop growth rate based on soil water supply and WR.
Crop water requirement satisfaction index	(Masupha and Moeletsi, 2020)

Rainfall can be estimated using gauging networks (Herold et al., 2016; Tapiador et al., 2012), but availability and quality of spatially-temporal data often is a concern in countries where resources are limited to maintain an observation network. A further constraint to the availability of rainfall data is that rain gauge networks often have a low gauge density with stations that are unevenly distributed in space with incomplete observation records by failure of automated recorders or observers (Behrangi et al., 2011). To arrive at consistent and spatial-temporal coherent time series, rainfall from stations often is spatially and temporally interpolated. The accuracy of spatially interpolated rainfall depends both on the gauge network density and the spatial coherence of the rainfall distribution (Beck et al., 2017a). *Spatial coherence* describes the cross-correlation between rainfall at different points in space and used to tell the uniformity of the rainfall distributions. Constraints on availability of rainfall data in crop growth simulations can be overcome by use of satellite rainfall estimates (SREs).

Use of SREs in crop growth simulations involves various methods including “forcing” (replacing meteorological input variables derived from remote sensing data), “calibration” (adjusting model parameters) and, “updating” (updating state variables e.g., soil moisture content, vegetative biomass whenever remote sensing data is available) (Ban et al., 2019). In this study SREs are evaluated as an alternative rainfall input data source in crop growth simulation. A key advantage of using SREs is the availability of consistent and spatially-temporally coherent rainfall data series with large spatial coverages (from continental to global) and high temporal resolutions (from monthly to 30 min) (Xianghu et al., 2014), whereas gauge networks provide point-based rainfall data at locations where gauges are installed.

With the current advancement of satellite remote sensing instruments, various gridded rainfall products have been developed with different design objectives, input data sources, spatial and temporal resolutions, spatial coverage, temporal spans, and latencies (Beck et al., 2017b). Four such products are selected for this study and include the Climate Prediction Center-MORPHing algorithm (CMORPH) (Joyce et al., 2004), the Climate Hazards group InfraRed Precipitation with Stations data (CHIRPS) (Funk et al., 2015), the African Rainfall Estimation algorithm (RFE) (Xie and Arkin, 1996), and the Multi-Source Weighted-Ensemble Precipitation (MSWEP) (Beck et al., 2017a) products. The concept behind these state-of-the-art SREs is information blending from passive microwave sensors with that from more frequent (but indirect) visible/infrared sensors. Microwave sensors are commonly mounted on orbiting satellites while visible/infrared sensors are commonly mounted on geostationary or low Earth-orbiting satellites, thus blending takes advantage of their complementary strengths (Behrangi et al., 2011; Joyce et al., 2004; Sun et al., 2018; Tapiador et al., 2012). Some SREs further consider active microwave and ground-based information for calibration (Funk et al., 2015; Huffman et al., 2007; Xie et al., 2017).

SREs exhibit significant uncertainty because of random and systematic errors (the latter described as bias (Smith et al., 2006)) as argued in Pan et al. (2010). Random errors tend to cancel out when estimates from the SREs are considered at large temporal windows (Jobard et al., 2011), unlike the SREs’ bias (Smith et al., 2006). Bias in these products originates from sensor calibration uncertainties, too low spatio-temporal

sampling frequencies, resampling or retrieval errors, amongst others (AghaKouchak et al., 2012; Maggioni et al., 2013); and manifests in inaccurate estimates of rainfall depths, occurrence, and intensities (Gumindoga et al., 2019; Habib et al., 2012; Yang and Luo, 2014). So, rainfall representations differ for each SRE product with different error distributions as affected by land surface conditions, latitude, season, and type of rainfall event (Hobouchian et al., 2017). When SREs serve as an input to a crop growth simulation, errors propagate to cause uncertainty in simulated outcomes (Luetkemeier et al., 2018; Ramarohetra et al., 2013). In the context of this study, *uncertainty* refers to aspects of error in simulated crop growth outputs due to SRE error propagation effects. Motivated by constraints of rainfall gauging networks and the potential of SREs to be used in crop growth simulation, there is a need to evaluate bias in SREs, their characteristics under various conditions, and the effects of bias propagation in simulating crop growth (e,g., Luetkemeier et al., 2018; Ovando et al., 2018; Ramarohetra et al., 2013; Reynolds et al., 2000). Studies in hydrological applications have explored how bias is affected by topography (dos Reis et al., 2017; Gao and Liu, 2013); by different seasons and arid environments (Tan et al., 2017; Yang and Luo, 2014) in reproducing rainfall amount, intensity, and occurrence (Dinku et al., 2011).

Whereas SREs are considered for simulation applications, consensus has been reached that SREs require bias correction and/or merging of SRE products to improve rainfall representation and their reliability (Bhattacharya and Solomatine, 2015; Haile et al., 2012). A first step is thus to assess bias in each SRE, their representation of soil water conditions for crop development and to confirm their usability in crop growth simulation, especially in rainfed agriculture. Studies by Beck et al. (2017b) and Behrangi et al. (2011) on the use of SREs in rainfall-runoff modelling show that bias varies spatially and temporally. For this study, the specific objectives are to i) evaluate the timing of SRE rainfall arrival at the onset of the crop growth season, ii) assess errors of the SREs in representing multi-day rainfall depths, iii) assess the representation of prolonged periods of dry days, (iv) evaluate rainfall detection occurrence errors for respective crop growth stages and v) to relate errors in rainfall representation to crop growth water requirements. This study explores if SREs are fit for use in crop growth simulation by providing an evaluation of SRE bias and bias error propagation into the water requirement satisfaction index with a focus on subsequent crop growth stages.

In this study, maize (*Zea mays* L.) is selected as the crop of interest since it is mostly grown in rainfed conditions. On a global scale maize is the third most important cereal and staple crop after wheat and rice (Chisanga et al., 2015). Water requirements at respective growth stages

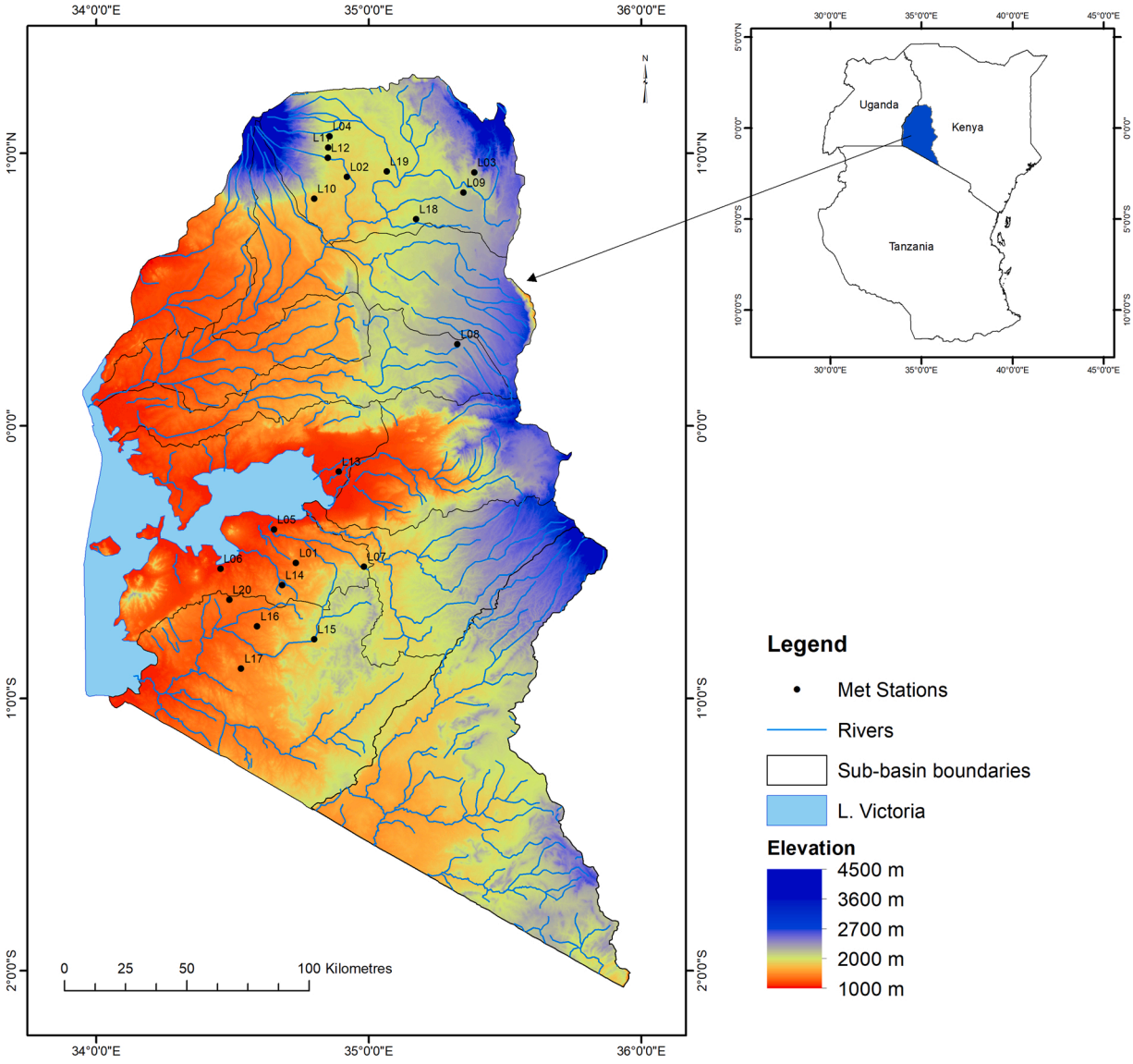

Fig. 1. The Lake Victoria basin of Kenya showing rain gauge station distribution for this study and topography derived from SRTM30 data.

are shown in Supplementary Materials section. Maize growth stages are the vegetative, silking (flowering), and reproductive stages (grain filling) (Sah et al., 2020) that are adopted in this study.

2. Materials and methods

2.1. Study area

The study area is in the Lake Victoria basin of Kenya (Fig. 1) that covers 43,368 km^2 (between 2° 05′ 00″ S to 1° 20′ 00″ N and 33° 55′ 00″ E to 36° 05′ 00″ E). The altitude range is 1079–4318 m above mean sea level. The hydrology of the area is defined by seasonal rivers. Tropical rain forests and a semi-dry climate dominate the basin.

Rainfall variability is typical with long rains from March to June and short rains from October to November, while the remaining months are characterized by intermittent dry spells. The rainfall distribution is bi-modal ranging between 1100 and 1700 mm yr^{-1}. The temperature varies between 12 and 26 °C. The soil texture ranges from loamy to clayey. Lowlands have predominant sandy–clay to silty–loamy soils whereas the upland has predominantly loamy soils.

The area supports approximately 13 million rural inhabitants that mainly practice subsistence farming. Rain-fed farming of mixed varieties of cereals, e.g., maize, as a staple food, inter-cropped with vegetables and potatoes is common. Subject to rainfall arrivals at the onset of the cropping season, farmers use seeding dates from early February through March to minimize the risk of crop failure. Average maize yield, which is susceptible to interannual rainfall variability and socio-economic constraints, is low ranging between 90 and 2500 kg ha^{-1} (Tittonell et al., 2008).

2.2. Gauged rainfall observations

Rainfall measurements are based on records from 20 rain gauge stations provided by the Agriculture and Climate Risk Enterprise Africa (ACRE Africa). All stations are automated weather stations (AWS). The data series have daily observations and are for the period between January 2012 and December 2018 except for two stations (Toro farm and Wiobiero) where records started in April 2012. An inventory of the stations is provided in Table 2. Some stations are affected by data gaps, but the available time series are of sufficiently long duration to serve the objectives of this study. Consistency and completeness checks of gauged rainfall time series were performed. The missing rainfall records were not gap-filled to avoid introducing possible errors in the gauged data series that serve as reference for the SREs. We note that none of these rain gauge stations have been used in tuning the algorithms for SRE products selected for this study.

Table 2
Rain gauge stations and data gaps for the period 2012–2018.

Station		Latitude [°]	Longitude [°]	Altitude [m]	Gaps [%]
ID	Name				
L01	Agore Sare S School	-0.50244	34.73319	1427	2.0
L02	Bubayi Farm, Saboti	0.91384	34.91988	1794	0.1
L03	Chebororwa ATC	0.92930	35.38760	2088	0
L04	Elgon Downs Farm, Kitale	1.06275	34.85658	1926	2.0
L05	Gendia H School	-0.38108	34.65257	1227	2.1
L06	Homa Bay Water Supply	-0.52472	34.45662	1157	9.3
L07	Kebabe Girls, Ikonge	-0.51694	34.98345	1914	0
L08	Keses DO	0.29961	35.32593	2241	0
L09	Kibogy Farm	0.85625	35.34804	2091	14.8
L10	Kikwamet farm, Sihendu	0.83347	34.80021	1776	1.4
L11	Kireka Farm	1.02134	34.85210	1913	15.8
L12	Lakitela Farm, Saboti	0.98343	34.85015	1912	0
L13	Lela Secondary School	-0.16790	34.89046	1156	0.1
L14	Mititi S School	-0.58472	34.68282	1512	0
L15	Nyamagwa Girls, Igare	-0.78348	34.80005	1850	1.8
L16	Nyarach Secondary School	-0.73605	34.59068	1438	14.7
L17	Sony Sugar Factory	-0.89038	34.53188	1500	0
L18	St Micheal Kipsombe S	0.75801	35.17365	1969	0
L19	Toro Farm Bubayi	0.93334	35.06674	1850	1.8
L20	Wiobiero S School	-0.63783	34.48917	1371	1.8

2.3. SRE products

The SRE products are described in Table 3. Time series for 2012–2018 were downloaded from respective repositories. The MSWEP product is only available up to October 2017.

2.3.1. CHIRPS 2.0

The CHIRPS product is a quasi-global (50°S–50°N) infrared cold cloud duration (CCD) based rainfall estimate (Funk et al., 2015). Main data sources for the CHIRPS algorithm include Climate Hazards Center's Precipitation Climatology (CHPClim), quasi-global geostationary IR satellite observations from CPC and NCDC, TRMM 3B42 product from NASA, atmospheric model rainfall fields from the NOAA CFSv2, and ground station rainfall data from various sources (Funk et al., 2014). The unbiased gridded CHIRP product generated from 0.05° CCD estimates is blended with ground station data to produce preliminary and final products with 2-days and 3-weeks latencies, respectively. According to the authors, this product is suitable for assessments in rainfall-data sparse locations that are dependent on convective rainfall. This study uses the daily CHIRPS Africa rainfall product at 0.05° spatial resolution. The datasets are available via https://data.chc.ucsb.edu/products.

2.3.2. CMORPH 1.0

The CMORPH product is based on a morphing approach where passive microwave (PMW) derived precipitation estimates and thermal infrared (TIR) brightness temperature from multiple sensors are blended to generate rain rates, which are then used to infer motion fields (Joyce et al., 2010). Tables 1 and 2 by Joyce et al. (2004) summarize these geostationary and PMW sensors. In generating the CMORPH dataset, ½h 8-km PMW rainfall estimates from various sensors are assembled and matched to TRMM TMI 2A12. IR data is then used to derive cloud system advection vectors (CSAVs) that spatially propagate forward and backward in time generating the combined PMW rainfall for every ½h. Both forward- and backward-propagated rainfall are subsequently inversely-weighted by the respective temporal distance from observed PMW rainfall producing the shape and intensity of precipitation at a location every ½h (Joyce et al., 2004).

The CMORPH estimates are adjusted using Global Precipitation Climatology Project (GPCP) data (Tramblay et al., 2016). The product is available at ½h (at 0.07°), 3 h (at 0.25°), and daily (at 0.25°) time steps. For this study, the time series of CMORPH rainfall images (2012–2018) at ½h and 0.07° resolution were selected and downloaded from www.ncei.noaa.gov/data through the GeoNETCAST ISOD toolbox of ILWIS 3.8.6 GIS software (https://52north.github.io).

2.3.3. MSWEP 2.2

Gauge-, satellite-, and reanalysis-based data are the inputs of the MSWEP product. MSWEP data cover the period from 1979 until 2017. It is available at 0.1° spatial resolution and 3 h, daily, and monthly temporal resolutions with full global coverage (Beck et al., 2019). The datasets are freely available via www.gloh2o.org. This study uses the 3 h version 2.2 of this product.

Table 3
Metadata of SREs used in this study.

Product	Input sources	Spatial		Temporal		Provider	References
		Coverage	Res.	Coverage	Res.		
CHIRPS 2.0	IR, MW, RG	≤ 50°N/S, land	0.05°	1981–NRT**	d	CHG	(Funk et al., 2015)
CMORPH 1.0	IR, MW	60°N/S, global	0.07°	1998–NRT**	½-h	NOAA-CPC	(Joyce et al., 2004)
MSWEP 2.2	RG, S, R, N	Global	0.1°	1979–2017	3-h	NOAA-CPC	(Beck et al., 2019)
RFE 2.0	IR, MW, RG, M	40°N/S, 20°W–55°E	0.1°	2001–present	d	NOAA-CPC	(Xie and Arkin, 1996)

(CHIRPS = Climate Hazards group InfraRed Precipitation with Stations data, CMORPH = Climate Prediction Center-MORPHing algorithm, MSWEP = Multi-Source Weighted-Ensemble Precipitation, RFE = African Rainfall Estimation algorithm, IR = infrared, MW = microwave imager, RG =rain gauges, S = satellite, R = reanalysis, N = radar, M = model, Res. = Resolution, land = coverage restricted to land surface, global = fully global coverage including ocean areas, NRT**= available until the present with a delay of several days, NRT*= available until the present with a delay of several hours, d = daily, h = hourly, CHG = Climate Hazards Group, NOAA-CPC= National Oceanic and Atmospheric Administration Climate Prediction Center)

2.3.4. RFE 2.0

RFE is a blended product based on daily Global Telecommunication System (GTS) rain gauge data and CCD derived from cloud top temperature – from Meteosat thermal infrared (TIR) data, Special Sensor Microwave/Imager (SSM/I), and Advanced Microwave Sounding Unit (AMSU). The three satellite estimates are linearly combined using a set of predetermined weighting coefficients minimizing the overall root mean squared error of the satellite estimates and then merged with GTS rain gauge data to produce daily, inherently corrected, rainfall estimates over Africa (Xie and Arkin, 1996). The RFE product is extensively used for food security monitoring or to supplement ground rainfall observations in East Africa by the famine early warning systems network (FEWSNET) (Jayanthi et al., 2013). It is available daily at a resolution of 0.1° and spatial extent of 40°N/S and 20°W–55°E.

2.4. SREs retrieval and pre-processing

The SREs were retrieved by extracting the daily rainfall estimates for the pixel that overlays a rain gauge station. In this study, sub-daily CMORPH and MSWEP images were aggregated to a daily temporal resolution, consistent with rain gauge observations, through a batch routine in ILWIS software. The incorporated customized ILWIS routine downloads the ½-h CMORPH and 3-h MSWEP from respective ftp sites; imports the files in ILWIS raster formats; creates map-lists of ½- and 3-h data and then mirror rotates them. It subsequently subsets the images and reprojects to the study area of interest and mosaic the ½-h CMORPH images to hourly equivalents. Finally, it aggregates the hourly CMORPH and 3-h MSWEP to daily totals. Nearest neighbour resampling (Cover and Hart, 1967) at a spatial grid size of 0.07° was used to arrive at directly comparable SRE's rainfall estimates. For reasons of brevity, detailed assessment on the pixel size and resampling method are not shown.

2.5. Evaluation of SREs in representing key rainfall characteristics for crop growth stage simulation

We used the point-to-pixel approach to compare point rainfall estimates of rain gauge observations (i.e., gauge funnel scale) and the four SREs at pixel scale for the period 2012–2018. This methodology has been widely used in assessing SREs (e.g., Bhatti et al., 2016; Cavalcante et al., 2020; Mekonnen et al., 2021; Worqlul et al., 2014) and assumes that SREs at pixel scale are representative counterparts of rain gauge station observations. Days with missing rainfall estimates at the rain gauge stations were considered as missing in the SRE time series for comparison.

The evaluation of the performances of the SREs in representing key rainfall characteristics was tailored to three crop growth stages: vegetative, reproductive, and ripening. The early days of the vegetative stage was further assessed as 'initial' adapting to the FAO classification (Savva and Frenken, 2002). Growth stage transitioning dates were kept unique for subsequent seasons and stations. The start of a long rainfall period indicated by the gauge was adopted as the start of the wet season and of the maize growing season. Rainfall occurrence detection errors of SREs were assessed using categorical error metrics, measuring frequency of (in)correct predictions of a model, and shifts in rainfall arrival dates. The estimation errors of the SREs were determined using the relative bias and crop water requirement satisfaction index (WRSI; Eq. (1)) indicating the potential crop water stress during the growing period. The ranking of the SRE products in detecting and estimating rain rates for crop growth stage simulation was based on a multicriteria analysis of the metrics as summarized in Table 4.

$$WRSI = \frac{AET}{WR} \times 100 \quad (1)$$

2.5.1. Assessment of rainfall onset day and dry spell

Rainfall onset day is determined as the first rainfall occurrence centered on March 1 with a minimum cumulative rainfall depth of 20 mm in 3 days with no dry spell larger than 10 days within the next 21 days in a growing season. The condition on dry spell length was added to ensure successful seeding. Long rains in the study area run from March through late October (e.g., Fig. 2). So, March 1 is used as the earliest date of seeding, and April 30 as the latest date when maize could be planted to ensure maturity before the end of the growing season. A *rainfall event* was considered as a day with rainfall above 0.85 mm. The 0.85 mm d^{-1} threshold is not only a practical way of implementing rainfall events 'above 1 mm d^{-1}' suggested by the World Meteorological Organization, but also harmonizes with the measurement accuracy of rainfall time series obtained from AWS for this study. Onset day as represented by each of the SREs denoted as S_o (in date) is determined and thereafter time shifts from rain gauge observed counterparts (G_o) as reference is calculated. So, a negative $S_o - G_o$ value indicates an early arrival by the SRE, otherwise a late arrival. *Dry spell* is taken as the number of days between two rainfall events, and thus, its length was used to indicate the longest number of consecutive days with a rainfall amount below 0.85 mm on each day within a growth stage, signifying periods of inadequate rainfall to moisten the soil for crop growth.

2.5.2. Assessment of rainfall occurrence

Bias in detecting rainfall occurrence by the SREs was assessed using

Table 4
Rainfall characteristics for crop growth stages and their related evaluation indices used in the analysis.

Rainfall characteristic	Crop growth stage	Evaluation index
Onset day	Early vegetative	Shifts in rainfall arrival dates
Occurrence	All the four growth stages (initial, vegetative, reproductive, and ripening)	Probability of detection, critical success index, and false alarm ratio
Rainfall depth	All the four growth stages	Relative bias and maize WRSI
Dry spell	All the four growth stages	Dry spell length

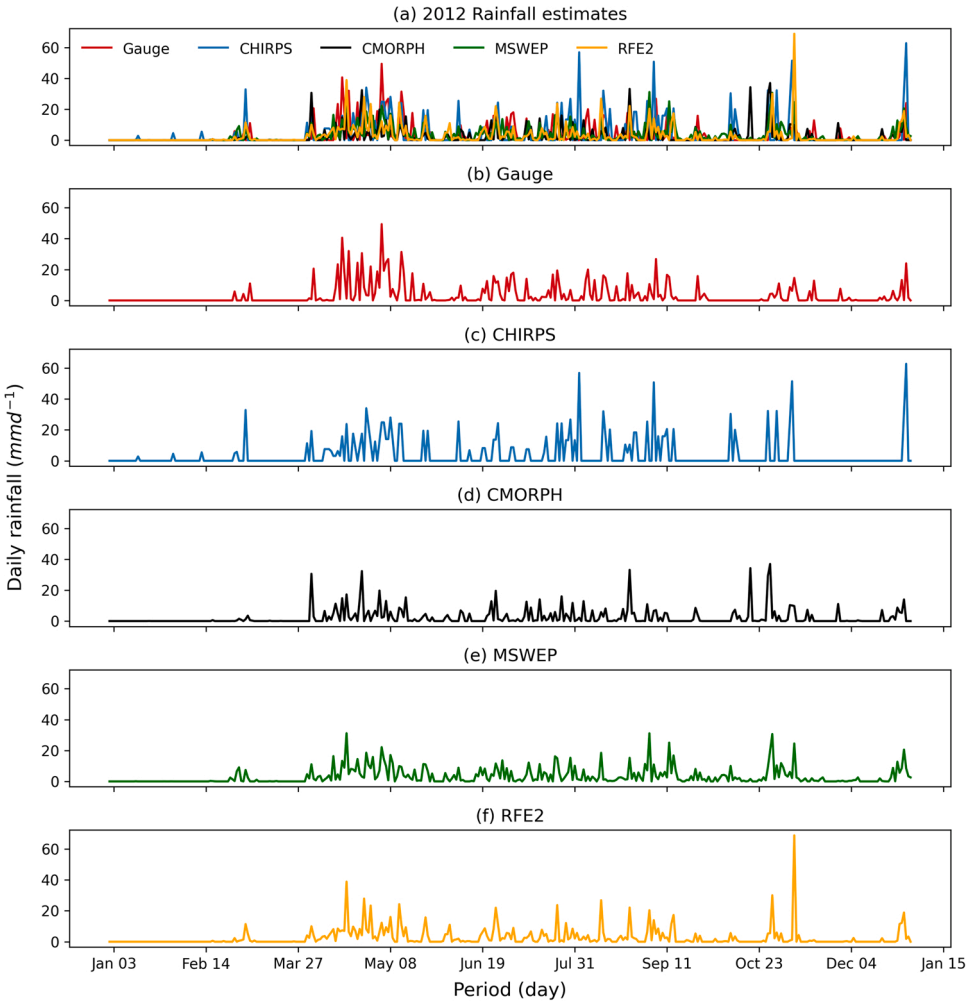

Fig. 2. Time series of 2012 daily rainfall (a) combined (b) gauged only and (c – f) satellite-based for pixel overlaying L03 station in Lake Victoria basin.

three categorical error metrics: the probability of detection (POD; Eq. (2)), false alarm ratio (FAR; Eq. (3)), and critical success index (CSI; Eq. (4)) detailed in Wilks (2006). A binary skill score (yes/no) was adopted to determine these categorical error metrics as per contingency Table 5.

The *POD* indicates correctly detected rainfall occurrence, *FAR* gives the proportion of falsely detected rainfall occurrence, and *CSI* indicates the fraction of the number of correctly detected rainfall occurrence by SREs. They range between 0 and 1.

$$POD = \frac{H}{H+M}, \quad \text{best} = 1, \text{worst} = 0 \tag{2}$$

$$FAR = \frac{FA}{H+FA}, \quad \text{best} = 0, \text{worst} = 1 \tag{3}$$

$$CSI = \frac{H}{H+M+FA}, \quad \text{best} = 1, \text{worst} = 0 \tag{4}$$

Table 5
Contingency table used to evaluate rainfall occurrence detection by the SREs.

	Rain Gauge Observations		
SREs	Yes	No	Total
Yes	Hit (H)	False Alarm (FA)	H + FA
No	Miss (M)	Correct Negative (CN)	M + CN
Total	H + M	FA + CN	

2.5.3. Assessment of rainfall depths

Rainfall depth was considered as the aggregated rainfall depth for a specific growth stage. The magnitude by which SREs deviate from rain gauge observed counterparts was evaluated using relative bias (Eq. (5)) and WRSI. Relative bias was selected as a measure of the systematic difference between SRE and rain gauge estimates relative to gauged estimates (Smith et al., 2006). A negative bias indicates underestimation by the SRE, a positive bias indicates overestimation.

$$Relative\ Bias\ [\%] = \frac{\sum_{i=1}^{N}(S_i - G_i)}{\sum_{i=1}^{N} G_i} \times 100\% \tag{5}$$

where S_i and G_i are satellite and gauge rainfall estimates (in mm) at day i, respectively; N is the total number of days.

The WRSI, as a measure of crop performance based on soil water availability to the crop during a growing season (Senay and Verdin, 2002), was used to assess the effects of soil water stress on crop growth. WRSI values were determined using a crop water balance model in Instat+ 3.37 software developed by Statistical Services Centre and originally available at www.ssc.rdg.ac.uk. The Instat+ statistical package was selected because of its modest input data requirement and being less sophisticated compared to a full crop growth model. Respective index values were estimated using daily rainfall, potential evapotranspiration (PET), soil water holding capacity (SWHC), and a crop coefficient (*Kc*) as inputs.

The SWHC values in Table 6, that indicate the maximum amount of water that a given soil can hold to serve crop growth, were obtained from the soil and terrain database for Kenya (KENSOTER) version 2.0 provided by ISRIC (International Soil Reference and Information Centre, 2004). The widely accepted FAO-56 Penman-Monteith method (Allen et al., 1998), that employs location-specific solar radiation, air temperature, relative humidity and wind speed, was used to compute PET in R-Instat (r-instat.org) software. Day of year averages of PET were used in cases where these input records were missing.

A crop coefficient was derived for each of the four maize growth stages considering a maize crop maturity of 180 days. Values were estimated based on the *Kc* approach developed by Allen et al. (1998). In this approach, *Kc* values for initial and ripening crop growth stages were linearly interpolated to generate intermediate *Kc* values for vegetative and flowering crop growth stages. The calculated values were then used to construct the *Kc* curve (Fig. 3).

The maize WRSI for a growing season was calculated as a ratio of *AET* to WR (in mm) for a specific station expressed in Eq. (1). The WR was calculated by multiplying *PET* by estimated *Kc* values following Eq. (6).

$$WR = PET \times Kc \tag{6}$$

AET representing the actual water depth that is lost from the soil water storage by evapotranspiration was estimated through the soil water balance method incorporated in Instat+. During a simulation, soil water content is obtained through a mass balance Eq. (7) where soil water is monitored in a volume defined by SWHC (a detailed description is in Masupha and Moeletsi, 2020).

$$SW_i = SW_{i-1} + P_i - AET_i \tag{7}$$

where, *SW* is soil water content, *P* is rainfall, and *i* is the daily time step.

The WRSI is calculated daily and the cumulative potential of growth stress by soil water shortage during the growing season is given at the end of the cropping season. An index value of 100 indicates no growth stress as the WR is fully satisfied by rainfall but decreases when rainfall is too low to satisfy the crop growth water requirement, that as such causes soil water stress to crop growth. Impact of rainfall deficit on maize crop growth was interpreted based on the WRSI classification in Table 7 after Masupha and Moeletsi (2020).

3. Results

Because inter-seasonal rainfall patterns differ and thus affect seasonal crop growth, cumulative rainfall received from the 20 rain gauge stations over the crop growing seasons of 2012–2018 is compared in Fig. 4. The figure shows that the cropping season of 2012 received most rain compared to other seasons, in particular during the critical crop growing days before the 200th day from the start of the growing season. The increase in the 2012 curve appeared to decline after the 200th day, closely matching that for 2013 and 2018. However, the 2012 cropping season exhibited the highest rainfall and thus also highest mean daily rainfall.

Further analysis of rainfall shows that 2015 and 2016 had the least accumulated rainfall and were considered as dry crop growing seasons. For critical crop growth days, the aggregated rainfall recorded over 2015 and 2016 was higher than for 2014 and 2017, with least rainfall for 2014. The mean daily rainfall in 2014 was lower than that of 2017 by 0.3 mm. In this study, 2012 and 2014 were the wettest and driest crop growing seasons, respectively.

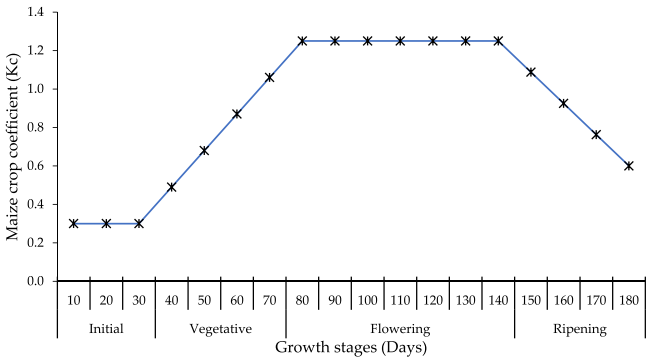

Fig. 3. Kc curve representing maize crop coefficients for each growth stage of a 180- day maturing maize crop in the Lake Victoria basin.

Table 7
WRSI classification scale indicating impact of rainfall deficit conditions on crop performance.

WRSI	Rainfall deficit classification	Crop performance description
100–80	No water stress	Good
79–70	Mild	Satisfactory
69–60	Moderate	Average
59–50	Severe	Poor
< 50	Extreme	Total crop failure

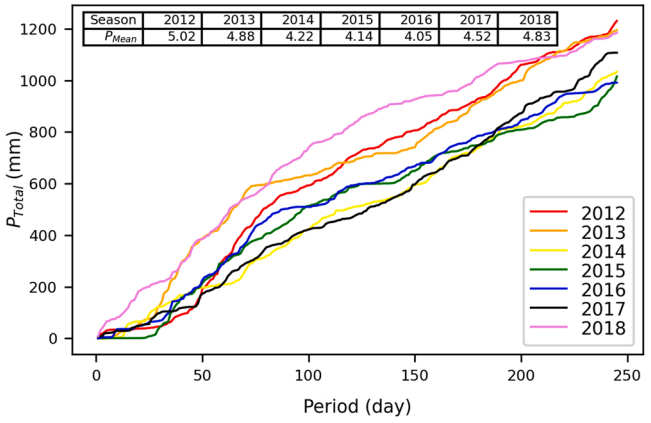

Fig. 4. Cumulative mean daily rainfall observed from the 20 stations in Lake Victoria basin for 2012–2018 cropping seasons. The cropping season runs from March 1 through October 31. The sub-set table indicates the mean values of daily rainfall during the cropping seasons.

3.1. Rainfall onset day representation

Fig. 5 shows the distribution of mismatch in marking the start of the wet season rains for each of the four SREs selected for this study. Any mismatch is considered bias that is specific to each SRE product.

Table 6
Soil water holding capacities (in cm m^{-1} of soil depth) used for the study.

Station ID	L01	L02	L03	L04	L05	L06	L07	L08	L09	L10
SWHC [cm/m]	19	7	7	10	11	14	23	9	9	7
Station ID	L11	L12	L13	L14	L15	L16	L17	L18	L19	L20
SWHC [cm/m]	10	18	12	11	11	9	11	13	13	15

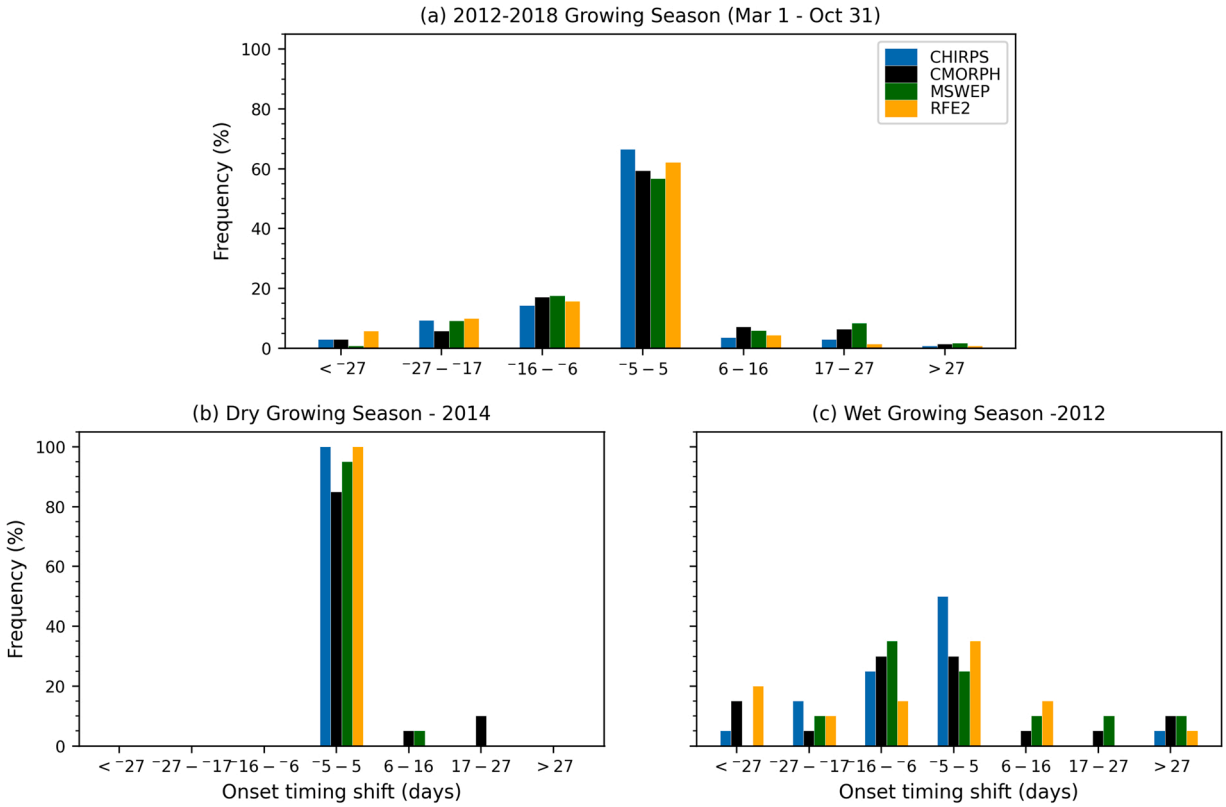

Fig. 5. Frequency of differences between rainfall arrival estimated by SREs and gauged observation as reference for (a) all the crop growing seasons of 2012–2018 (March 1 – October 31), (b) dry crop growing season and (c) wet crop growing season in Lake Victoria basin. MSWEP series only covers the 2012–2017 seasons. The negative and positive values define early and late rainfall arrivals in days, respectively indicated by the SRE with respect to gauged observation as reference.

Whereas Fig. 5 shows mismatch for all cropping seasons (2012–2018), we refer to the attached Supplementary Materials section for assessments of each year. Most differences in Fig. 5a do not exceed 5 days (i.e., > 54% for each SRE). Misrepresentation of the rainfall onset by SREs was found to be skewed towards early arrivals (with shifts ranging between –6 and –27 days dominating). It can be seen on the extremes that an SRE could miss a rainfall onset by indicating an early or late arrival up to a shift of more than 27 days.

Fig. 5b for the dry growing season 2014 shows that the onset timing differences were dominantly within ± 5 days with infrequent late arrivals indicated by CMORPH and MSWEP. For the wet growing season (Fig. 5c), the differences were fairly distributed within ± 27 days during a wet cropping season.

Whereas no SRE was most preferred in representing rainfall onset, RFE2 showed the least onset error, followed by CHIRPS. The latter consistently showed no rainfall arrivals later than the gauged counterparts, except during wet cropping seasons, e.g., 2016 and 2017. MSWEP and CMORPH products mainly indicated delays in rainfall arrivals.

3.2. Bias in representing dry spell length

Except for initial and ripening stages, the box-whisker plot in Fig. 6 shows that all SREs differ with gauged observations in representing dry spell lengths. At least 50% of CHIRPS estimates showed less than five days dry spell lengths that was also reported in gauged observations during the initial stage, a similar pattern by CMORPH during ripening. Results indicate larger interquartile ranges during the flowering stage.

The median and mean dry spell lengths recorded by CHIRPS are consistently higher than gauged observations throughout the four growth stages. In contrast, however, the median of the product is aligned with gauged observations for the initial growth stage. Medians from the other SREs were consistently lower than gauged observations for all

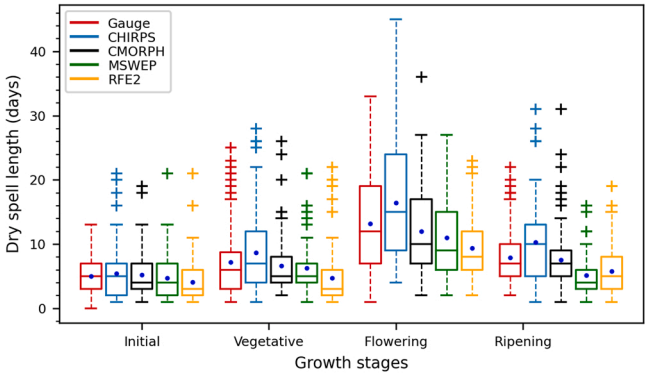

Fig. 6. Distributions of dry spell lengths from rain gauges and SREs for each crop growth stage within a particular cropping season covering the 2012–2018 period. A single box-whisker represents a series of seven years from 20 rain gauge stations in the Lake Victoria basin indicated by an SRE product or gauged observation. In the box-whisker plots, a box represents the 25th and 75th percentiles, with the line in the box as the median (50th percentile) while the whiskers indicate the extreme values (5% and 95%). The crosses indicate the outliers. The blue dot in the box shows the mean value.

growth stages. Compared to other SREs, CHIRPS exhibited larger variations in dry spell length that increased in magnitude towards later growth stages. Except for the ripening growth stage, RFE2 consistently indicated the lowest mean and median dry spell lengths. All the SREs showed a misfit in representing dry spell length reported at the gauge, possibly owing to the inability of SREs to indicate the minimum dry spell lengths from the gauge. Except for MSWEP during the vegetative stage, the SREs exhibited a skewed spread towards long dry spell lengths that was also reported in gauge observations. While all SREs had outliers at

each growth stage, CMORPH and MSWEP had a larger number during vegetative and ripening stages. The SREs misrepresented the lowest dry spell length, except RFE2 during the initial stage.

All SREs except RFE2 could fairly show agreement with gauged observations on capturing the long dry spells during the initial crop growth stage. For the vegetative stage, only CMORPH results agreed with gauged observations. However, no alignment was seen at later crop growth stages (e.g., flowering and ripening) for all SREs.

Fig. 7 shows a comparison of the bias of each SRE in representing the dry spells for the four crop growth stages with respect to the rain gauge observed counterparts. Most underestimations and overestimations do not exceed three days (i.e., > 40% by each SRE in each growth stage). Results show that the differences are less frequent during the early growth stages (i.e., initial and vegetative) but increase later. This is consistent with the short dry spell lengths seen during the initial and vegetative growth stages in Fig. 6. CHIRPS tend to overestimate dry spell lengths for each growth stage. RFE2 and MSWEP show underestimations for all four growth stages. While CMORPH show underestimations during the vegetative and flowering stages, no distinct response is seen during the initial and ripening stages. Based on these distributions and SRE biases, CHIRPS and RFE2 are least preferred for representing dry spell lengths. Whereas CMORPH show a better performance than the other SREs and is closely challenged by MSWEP, it is prone to outliers.

3.3. Performance of SREs in detecting rainfall occurrence

Rainfall occurrence detection for different crop growth stages is shown in Fig. 8, further results are available in the Supplementary Materials section. Results of a comparison between dry and wet cropping seasons are shown in Fig. 9. Results show a decrease in median values of POD from early to later growth stages, for all SREs, with an increase only realized at later stages. Specifically, MSWEP showed the best detection capability with median POD values of 0.9 and 0.8 for initial and flowering stages, respectively. Compared to other SREs, this product had the highest correctly detected rainfall occurrence during the wet cropping season (Fig. 9b). As for the rainfall detection pattern exhibited by MSWEP, POD median values for RFE2 were consistently higher than those of CHIRPS and CMORPH.

The detection capability of the SREs significantly dropped during dry cropping seasons. The median POD value of RFE2 was 0.95 in the wet cropping season 2017 compared to 0.85 in the dry cropping season 2014. However, RFE2 still outperformed the other SREs in detecting rainfall during the dry cropping season for all except the flowering stage. Irrespective of seasonal variations, CHIRPS showed weak results in detecting rainfall events. During the dry cropping season, rainfall detection of the products showed a median POD above 0.25 for the flowering stage. Larger variations of POD values were seen in CHIRPS compared to other SREs. Comparison based on the fraction of correctly detected rainfall events shows that MSWEP and CHIRPS reported the best and worst median CSI values, respectively. As for the POD pattern, the CSI values deteriorated as the number of rainy days increased.

In terms of falsely detected rainfall, CHIRPS generally exhibited the best results. This contradicts the other results on POD and CSI. The median FAR values of this product were 0.2 and 0.35 for early and late crop growth stages, respectively. MSWEP produced the weakest detection skill compared to the other SREs with median FAR values ranging between 0.25 and 0.45. We found a large spread in FAR values during the late growth stages, particularly in CHIRPS. Compared to other SREs, results suggest that CHIRPS recorded the largest spread in FAR (Fig. 9a) that conflicts with its best performance in all but the flowering stage. Except for later crop growth stages, all the SREs had a better performance during a wet than a dry cropping season.

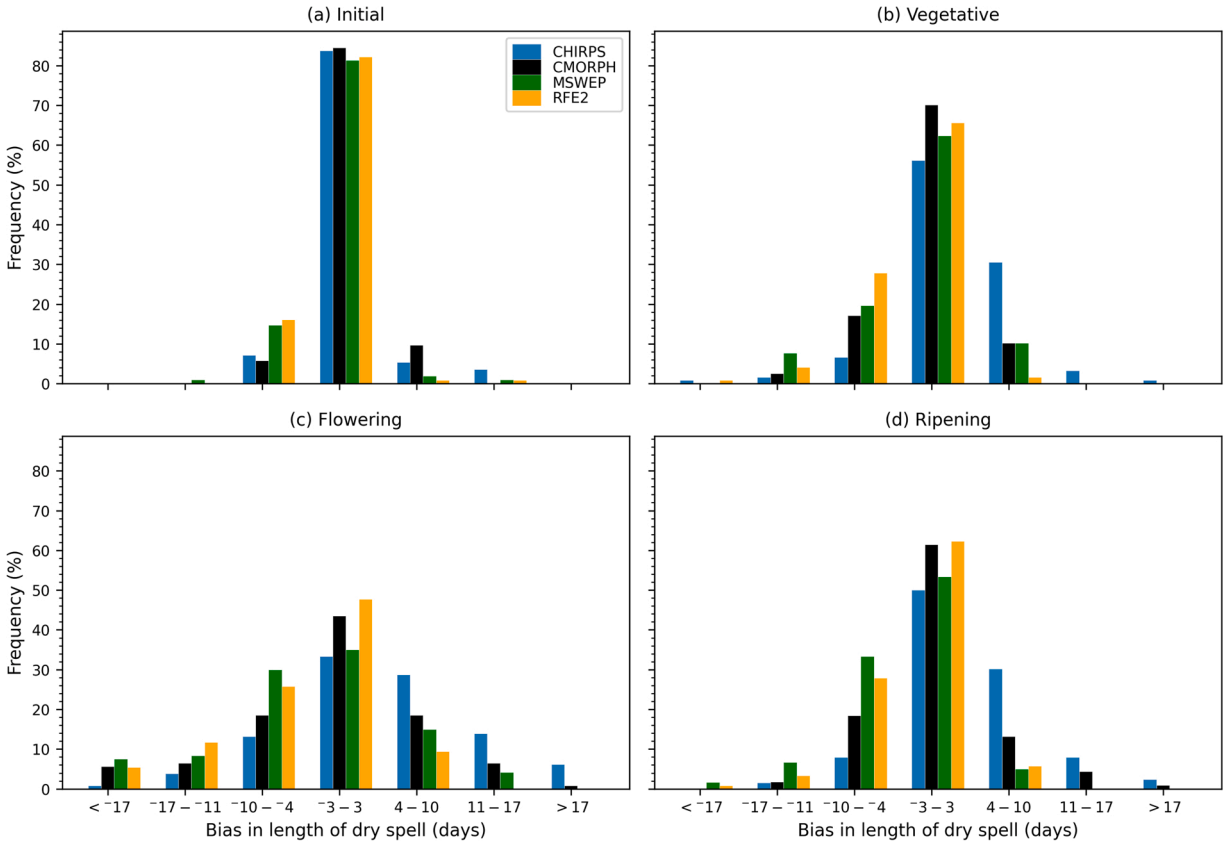

Fig. 7. Bias in representing dry spell durations by satellite rainfall products with respect to gauged observation as reference for the crop growing period of 2012–2018 (March 1 – October 31) in Lake Victoria basin. MSWEP series only covers the 2012–2017 cropping seasons. The negative and positive values denote under- and over-estimations, respectively, by an SRE.

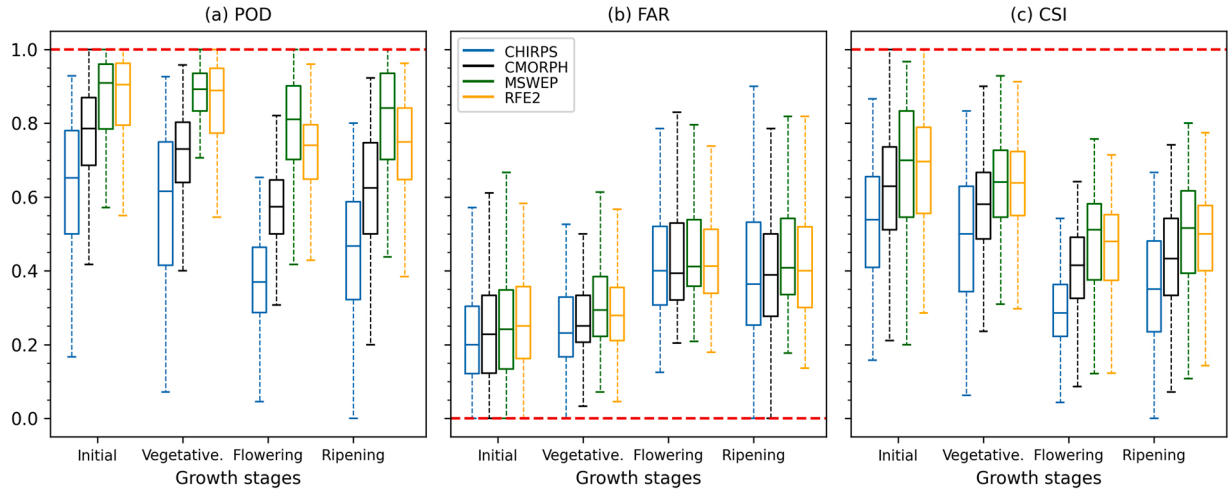

Fig. 8. Detection of rainfall occurrence by SRES for each crop growth stage within a particular crop growing season accumulated across 2012–2018 periods using box-whisker plots of POD, FAR and CSI. A single box-whisker represents a series of seven years from 20 rain gauge stations in the Lake Victoria basin indicated by an SRE product. In the box-whisker plots, a box represents the 25th and 75th percentiles, with the line in the box as the median (50th percentile), while the whiskers indicate the extreme values (5% and 95%). The red dotted lines indicate the optimal value of POD, FAR and CSI.

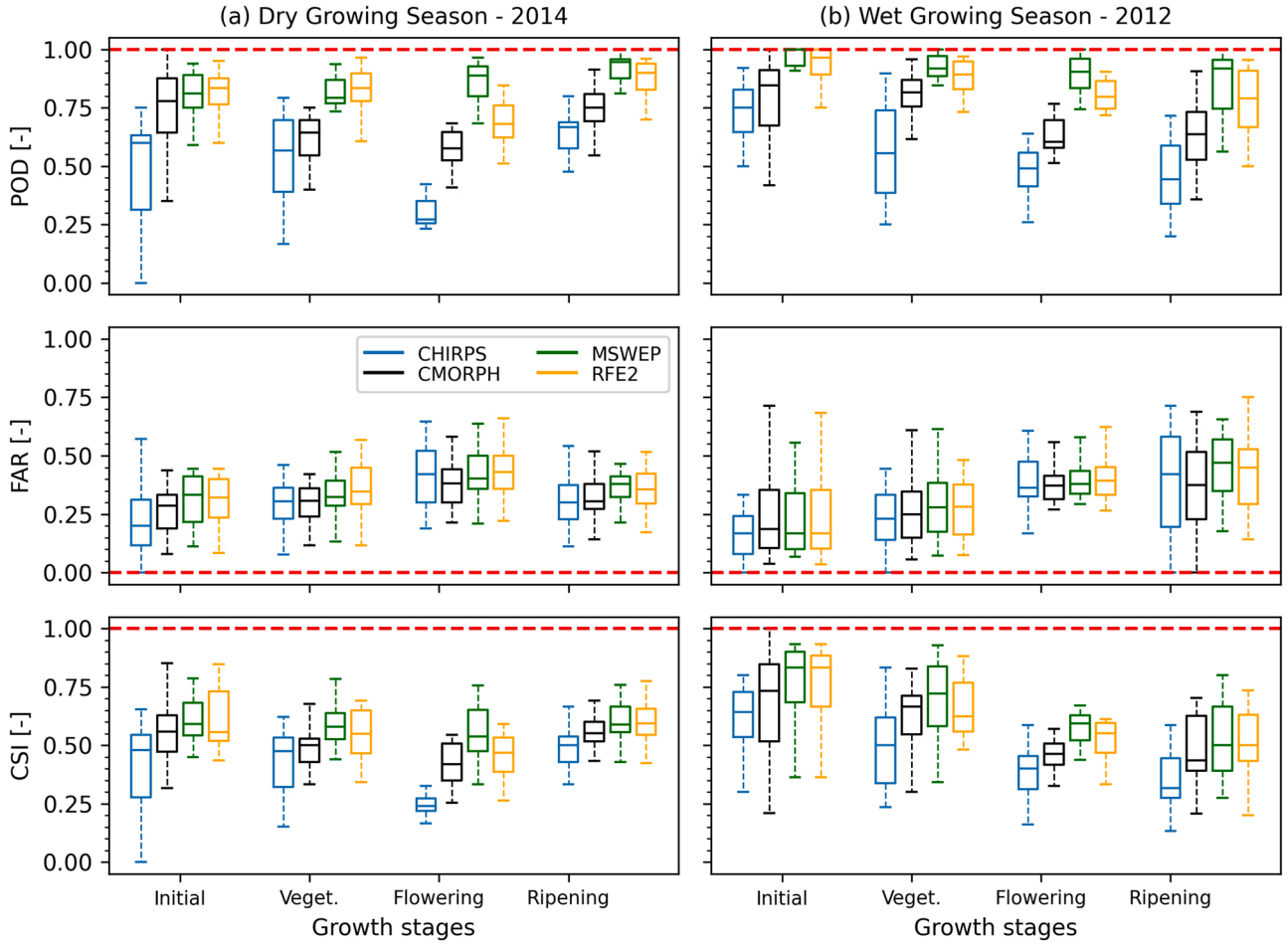

Fig. 9. Comparison of rainfall occurrence detection by SRE for each crop growth stage during (a) dry crop growing season and (b) wet crop growing season using box-whisker plots of POD, FAR and CSI from 20 rain gauge stations in the Lake Victoria basin. The red dotted lines indicate the optimal value of POD, FAR and CSI.

In general, detecting rainfall events by the SREs deteriorated as the cropping season progressed. This suggests good performance by SREs to validate their usability in crop growth simulations because early growth stages are the most critical for crop growth analysis.

3.4. Bias in rainfall depth

Fig. 10a compares the systematic differences in rainfall depths indicated by the SREs with respect to gauged counterparts (2012–2018)

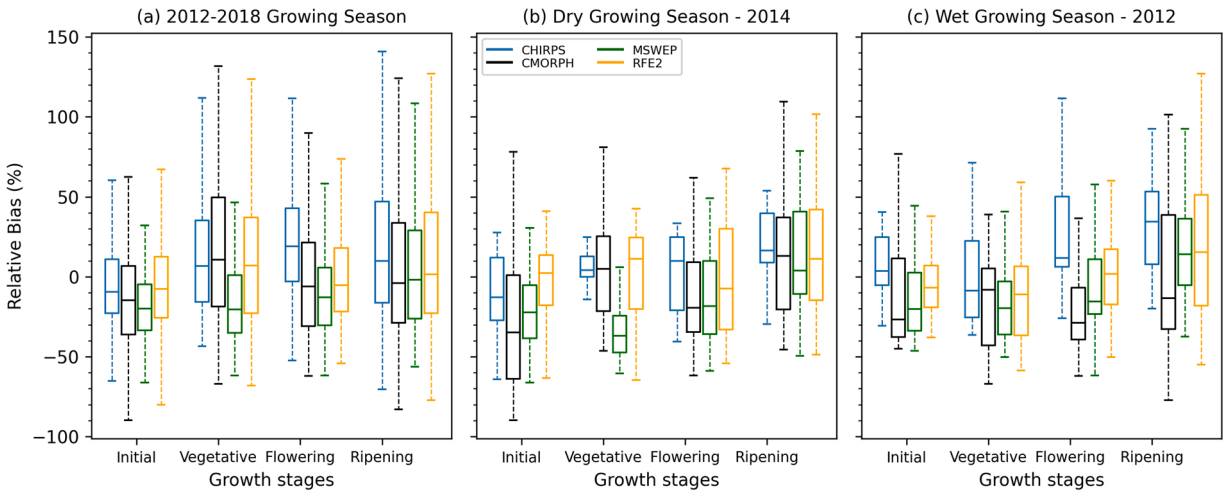

Fig. 10. Relative bias in rainfall depths estimated by SREs with respect to gauged estimates as reference (a) across all 2012–2018 crop growing seasons (b) dry crop growing season and (c) wet crop growing season covering 20 stations in the Lake Victoria Basin. The values lower than zero indicate an underestimation of rainfall depths, and the values higher than zero indicate overestimation by the SRE.

for different crop growth stages. Further results are in the Supplementary Materials section. SREs underestimated rainfall depths during the initial growth stage based on median value of relative bias. A similar result is shown for the wet (2012) and dry (2014) cropping season (Fig. 10(b) and (c) respectively). When products are evaluated for the least bias during the initial growth stage, CHIRPS and RFE2 are preferred despite some underestimations. Only CHIRPS shows underestimation during flowering and ripening stages.

An assessment of the individual SREs over the cropping season shows that the underestimation by SREs tends to reduce in the vegetative stage but becomes large in the flowering stage. The vegetative growth stage, unlike other stages, experienced overestimates as shown by the SREs except for MSWEP. Consistent underestimation of rainfall depths in MSWEP is noticed throughout three growth stages. For the ripening stage the product occasionally overestimates gauged counterparts in both dry and wet cropping seasons. MSWEP showed the least interannual spread despite its consistent underestimation, while CMORPH and CHIRPS indicated the largest spread of relative bias during the early and late growth stages, respectively.

Except for the 2017 cropping season, we found the least difference in rainfall depth between gauges and SREs during the initial and vegetative crop stages. This difference increases during the flowering and ripening stages. A similar performance pattern is noticed during dry and wet cropping seasons for all but the vegetative growth stage, where underestimation by the SREs is common during a wet cropping season, and the opposite is valid for a dry cropping season.

Further analysis on soil moisture availability for crop growth at different growth stages was carried out using WRSI. Table 8 shows the frequencies of different water stress levels (see definitions of episodes in Table 7) based on the WRSI for each growth stage represented by each SRE. For all SREs, simulated crop water requirement was met for the initial growth stage. For the earliest stages of crop growth, any bias in estimated rainfall did not result in shortage of soil water. It appeared that the net effect of bias in rainfall onset, rainfall occurrence and rainfall depth did not cause a bias propagation effect resulting in soil water stress conditions over respective crop growing windows. This is despite crops sensitivity to soil water at shallow depths for a shallow rooting depth. Index values decrease for vegetative, flowering, and ripening stages, with CMORPH recording the smallest value of 76.8 compared to the gauged counterpart at 75.9. As illustrated in the table,

Table 8
Descriptive statistics comparing the WRSI from different rainfall products and gauged rainfall for different crop growth stages over 2012–2018 cropping seasons across 20 stations in Lake Victoria basin.

GS	Product	Minimum	Mean	Std. Dev	Frequency of water stress degree levels (%)				
					No	Mild	Moderate	Severe	Extreme
Initial	**Gauge**	**94.32**	**99.63**	**0.73**	**100**	**0**	**0**	**0**	**0**
	CHIRPS	94.73	99.67	0.81	100	0	0	0	0
	CMORPH	92.32	99.41	1.28	100	0	0	0	0
	MSWEP	93.99	99.49	1.09	100	0	0	0	0
	RFE2	93.08	99.67	0.96	100	0	0	0	0
Vegetative	**Gauge**	**75.95**	**98.72**	**2.58**	**99.92**	**0.07**	**0**	**0**	**0**
	CHIRPS	82.77	98.87	2.31	100	0.00	0	0	0
	CMORPH	76.84	98.06	3.58	99.42	0.17	0	0	0
	MSWEP	79.17	98.19	2.86	99.96	0	0	0	0
	RFE2	78.87	98.90	2.49	99.97	0.02	0	0	0
Flowering	**Gauge**	**43.83**	**86.71**	**12.28**	**72.36**	**14.00**	**7.62**	**1.94**	**0.42**
	CHIRPS	48.61	88.17	11.63	75.72	13.26	5.81	1.45	0.17
	CMORPH	36.96	85.21	13.12	67.07	16.29	9.38	2.64	0.89
	MSWEP	45.08	81.91	12.43	57.81	19.26	13.34	3.61	0.25
	RFE2	45.51	86.30	12.79	69.70	15.65	7.24	3.06	0.51
Ripening	**Gauge**	**25.01**	**67.60**	**16.12**	**23.25**	**18.85**	**19.27**	**16.61**	**14.76**
	CHIRPS	29.92	70.99	15.97	29.74	18.81	20.60	12.78	11.17
	CMORPH	31.00	64.56	14.96	16.03	18.93	21.63	21.35	16.55
	MSWEP	30.77	60.51	12.87	7.36	16.16	23.66	24.24	22.66
	RFE2	33.40	66.49	14.86	16.77	20.56	24.01	18.93	13.95

CMORPH overestimated the frequency of mild water stress episodes compared to the rain gauge while the other SREs showed underestimations (i.e., CHIRPS and MSWEP missing to capture the episodes) in the vegetative stage.

Results show that the bias of SREs in representing severe and extreme water stress episodes was more frequent in the ripening than flowering stages. CMORPH, followed by RFE2, overestimated the frequency of extreme water stress episodes compared to gauged counterparts for the flowering stage. In contrast, CHIRPS followed by MSWEP showed underestimations. Total crop failure indicated by crop growth simulations applying the SREs would probably be expected at this stage. Except for CHIRPS, all SREs overestimated the frequency of severe water stress episodes. MSWEP, followed by CMORPH, overestimated the frequency of extreme water stress episodes by 7.9 and 1.8 per cent, respectively, during the ripening stage. CHIRPS and RFE2 showed underestimations of 3.6 and 0.8 per cent, respectively, for this growth stage.

4. Discussion

This study assessed SREs in representing rainfall characteristics meant for crop growth simulation at different crop growth stages. This study found that most differences in marking the start of the wet season rains by SREs with respect to gauged counterparts do not exceed five days. The representation of the onset day by the SREs suggests applicability of SREs as input in crop growth simulation. Whereas some skewness in misrepresentation of onset days by SREs is shown towards early arrivals, a possible explanation might be the false rains that are indicated by SREs.

Additionally, the late arrivals can be associated with SREs failing to detect rainfall occurrence reported at the rain gauges. The missed and falsely detected rainfall also may cause the difference noticed in the representation of the onset days by SREs during dry and wet growing seasons. The wide variation in timing of rainfall arrival by the SREs, and the inability to identify a preferred SRE product based on onset day representation implies that SREs must be validated with gauged observations.

Incorrect timing of seeding data in crop growth simulation (due to incorrect rainfall arrival as indicated by an SRE), can lead to error propagation that affects simulation results. In cases of dry direct seeding followed by delayed rainfall arrival by SREs input in the crop growth simulations, a reseeding would be required because seeds may fail to emerge due to soil moisture deficit intolerance. Even if the seeds emerge utilizing antecedent soil moisture, they may quickly die, leading to total crop failure in the simulation process. SREs indicating early arrival of rains can be beneficial, but the seedling depends on subsequent rainfall patterns (both in distribution and amounts).

This study compared the distribution and SRE's bias on detecting dry spell lengths (Fig. 6 and Fig. 7). Larger interquartile ranges during the flowering stage were found, suggesting that the dry spell length has more interannual variability during this stage. Another finding is that CHIRPS showed large spreads that increased towards later growth stages (i.e., flowering) in representing dry spell length, besides consistently overestimating the means and medians compared to gauged counterparts. Following Guo et al. (2015) and Yadav et al. (2013), maize crop is sensitive to moisture stress at the flowering stage. So, forcing a crop growth model with CHIRPS rainfall could lead to simulated results indicating increased days to flowering, reduced growth and biomass due to reduced soil moisture from long dry spells. This aspect of SRE performance makes the CHIRPS product less preferred to other SREs based on dry spell representation. The infrequent bias in representing the dry spell lengths during initial and vegetative stages that increased in later stages is possibly caused by more frequent rainfall events at the start of cropping seasons. Dry spell appeared to be more frequent during later stages of crop growth than early stages. This is partly in line with Fall et al. (2021) who showed dry spell occurrence is more frequent at the start and end of rainy seasons in Senegal. It should be noted that dry spell assessment was limited to SRE's bias. However, further insights on the characteristics and extent to which they influence soil moisture for crop growth can be derived by using different dry spell indices (e.g., based on accumulated rainfall during a specified period or intensities).

MSWEP, followed by RFE2, exhibited the best results in detecting rainfall events. As noted in previous studies (e.g., Beck et al., 2019; Xie and Arkin, 1996), both algorithms integrate rain gauge station data and this can explain the exhibited performance. However, we could not verify gauged observations for the current study in these two SREs blending procedures. RFE2′s best results in detecting rainfall events during the dry cropping season for all except the flowering stage can be attributed to the sensitivity of the algorithm, as an infrared-based SRE that incorporates a temperature threshold, to low rainfall rates that are predominant during dry periods (Mekonnen et al., 2021). RFE2 is also extensively used for food security monitoring or to supplement ground rainfall observations in East Africa by FEWSNET (Jayanthi et al., 2013). Falsely detected rainfall and large variations in POD values were frequent in CHIRPS, particularly in later growth stages. This weak performance indicates the product is less skillful in detecting extreme low and high rainfall depths experienced during early and late growth stages, respectively. Since at later growth stages, crops are at an advanced stage of development, effects of the poor performance might be insignificant when a crop growth simulation uses CHIRPS rainfall as input, but simulation results are affected regardless. According to Funk et al. (2015), CHIRPS is a blended-product of CHIRP and rain gauge stations data. Therefore, a better rainfall detection capability would be expected than other SREs, which was not the case in this study. A probable reason for this could be that only four rain gauge stations in and around the Lake Victoria basin were included in the blending procedure by product providers. Thus, the study recommends incorporating omitted rain gauge stations data in blending procedures, where applicable, as one approach to improve SREs detection capabilities. A complete list of gauged observations that the CHIRPS algorithm uses each month is accessible at the Climate Hazards Center data repository (https://data.chc.ucsb.edu). The weaker rainfall detection capability shown by SREs as the cropping season progressed might not be so critical for crop growth simulation because soil moisture becomes less critical towards the later growth stages. However, other approaches to improve SREs algorithms in detecting rainfall events are essential. Some improvement might result from merging the SREs to capitalize on their strengths for crop growth simulation. SREs generally performed better during a wet than a dry cropping season. This is consistent with previous findings (e.g., Dinku et al., 2011; dos Reis et al., 2017; Tan et al., 2017; Yang and Luo, 2014) evaluating rainfall products over different seasons and arid environment and concluded that they are season dependent.

Furthermore, bias in rainfall depths varied per SRE with no product showing a unique pattern of underestimation or overestimation in each crop growth stage. However, we found the least SREs bias in rainfall depths during early crop growth stages that deteriorated at later stages. MSWEP and CMORPH, respectively, showed the least and highest interannual spreads. From a perspective of a crop growth stage sensitivity to soil moisture deficits, it is reasonable to argue that the SRE's rainfall depth bias at later growth stages can be expected not to cause significant uncertainty in a crop growth simulated output when forced with SREs rainfall. SRE's bias in representing severe and extreme water stress episodes was found more frequent during the ripening than flowering stages in relating errors in rainfall representation to crop growth water requirements. Though extreme and severe water stress episodes are harmful to crop growth in simulations, the indicated bias frequencies during ripening pose an insignificant constraint to crop growth than it would during the initial stages. WR calculated based on estimates from all the SREs was satisfactory at the initial growth stages with insignificant biases, which decreased from the vegetative stage. The possible reason is that the WRSI values were determined at the onset of the cropping season when rainfall was considered sufficient to support crop growth. The overestimations of frequency of extreme water

stress episodes during the flowering stage by CMORPH could be linked to its performance in detecting dry spell lengths. As such, crop growth simulations forced with CMORPH rainfall might expect frequent episodes of soil moisture deficits and possible total crop failure during the flowering stage. In this same growth stage, CHIRPS and MSWEP underestimated severe water stress episodes.

These findings suggest that further testing and assessments on use of SREs in crop growth simulation is needed to assess how crop growth indicators such as leaf area index, bio-mass production and crop yield are affected. The study demonstrated that i) no SRE is most preferred for representing rainfall onset; ii) CMORPH showed the best performance in detecting dry spell lengths, iii) MSWEP, followed by RFE2, produced the best results in detecting rainfall events, and iv), MSWEP and CMORPH exhibited the least and highest interannual spreads in SRE's rainfall depth bias, respectively meant for crop growth simulations in Lake Victoria basin. Finally, CMORPH and RFE2 overestimated the frequency of extreme water stress episodes during flowering as a critical growth stage, whereas CHIRPS and MSWEP showed underestimations in relating SRE's errors representation to crop water requirement. This suggests that SREs require bias correction and/or an ensemble approach that capitalizes on best aspects of all the SREs to get one merged product that improves rainfall representation and reliability for crop growth simulations.

5. Conclusions

In this study, the bias of four SREs (CHIRPS, CMORPH, MSWEP, and RFE2) in representing multi-day rainfall onset, rainfall depths, dry spells, and rainfall occurrence for different crop growth stages was assessed. The evaluation focused on relating the bias in rainfall representation by SREs to crop water requirements for crop growth simulation. The findings indicate that the timing of rainfall arrival by the SREs widely varies. Regardless of the product, larger interannual variability exists in representing dry spell lengths during the flowering stage, with CMORPH and CHIRPS showing the best and weakest results. The SREs generally performed better during a wet than a dry cropping season in representing rainfall depths, detecting rainfall events and dry spell lengths, but their performance worsened as the cropping season progressed.

This study provides an assessment of the usability of SREs in crop growth simulation while focusing on their bias in different crop growth stages, where previous efforts focused on the entire cropping period. A detailed physically based crop growth modelling approach is recommended to provide information on how crop growth is affected when SREs are used instead of in-situ rainfall estimates.

Declaration of Competing Interest

The authors declare that they have no known competing financial interests or personal relationships that could have appeared to influence the work reported in this paper.

Acknowledgements

This research was funded by Nuffic (The Netherlands) through the Netherlands Fellowship Programme (NFP), and we greatly appreciate their support.

Appendix A. Supporting information

Supplementary data associated with this article can be found in the online version at doi:10.1016/j.agwat.2021.107204.

References

AghaKouchak, A., Mehran, A., Norouzi, H., Behrangi, A., 2012. Systematic and random error components in satellite precipitation data sets. Geophys. Res. Lett. 39. https://doi.org/10.1029/2012GL051592.

Ali, M., Mubarak, S., 2017. Effective rainfall calculation methods for field crops: an overview, analysis and new formulation. Asian Res. J. Agric. 7, 1–12. https://doi.org/10.9734/ARJA/2017/36812.

Allen, R.G., Pereira, L.S., Raes, D., Smith, M., 1998. Crop Evapotranspiration (guidelines for computing crop water requirements), FAO Irrigation and drainage paper 56. Food and Agriculture Organization of the United Nations, Rome, Italy.

Ban, H.-Y., Ahn, J.-B., Lee, B.-W., 2019. Assimilating MODIS data-derived minimum input data set and water stress factors into CERES-Maize model improves regional corn yield predictions. PLoS One 14, 0211874. https://doi.org/10.1371/journal.pone.0211874.

Beck, H.E., van Dijk, A.I.J.M., Levizzani, V., Schellekens, J., Miralles, D.G., Martens, B., de Roo, A., 2017a. MSWEP: 3-hourly 0.25° global gridded precipitation (1979–2015) by merging gauge, satellite, and reanalysis data. Hydrol. Earth Syst. Sci. 21, 589–615. https://doi.org/10.5194/hess-21-589-2017.

Beck, H.E., Vergopolan, N., Pan, M., Levizzani, V., van Dijk, A.I.J.M., Weedon, G.P., Brocca, L., Pappenberger, F., Huffman, G.J., Wood, E.F., 2017b. Global-scale evaluation of 22 precipitation datasets using gauge observations and hydrological modeling. Hydrol. Earth Syst. Sci. 21, 6201–6217. https://doi.org/10.5194/hess-21-6201-2017.

Beck, H.E., Wood, E.F., Pan, M., Fisher, C.K., Miralles, D.G., van Dijk, A.I.J.M., McVicar, T.R., Adler, R.F., 2019. MSWEP V2 global 3-hourly 0.1° precipitation: methodology and quantitative assessment. Bull. Am. Meteorol. Soc. 100, 473–500. https://doi.org/10.1175/BAMS-D-17-0138.1.

Behrangi, A., Khakbaz, B., Jaw, T.C., AghaKouchak, A., Hsu, K., Sorooshian, S., 2011. Hydrologic evaluation of satellite precipitation products over a mid-size basin. J. Hydrol. 397, 225–237. https://doi.org/10.1016/j.jhydrol.2010.11.043.

Bhattacharya, B., Solomatine, D., 2015. Bias correction of satellite-based rainfall data. Geophys. Res. Abstr. EGU Gen. Assem. 17, 2015–12502.

Bhatti, H., Rientjes, T., Haile, A., Habib, E., Verhoef, W., 2016. Evaluation of bias correction method for satellite-based rainfall data. Sensors 16, 884. https://doi.org/10.3390/s16060884.

Bombardi, R.J., Pegion, K.V., Kinter, J.L., Cash, B.A., Adams, J.M., 2017. Sub-seasonal predictability of the onset and demise of the rainy season over monsoonal regions. Front. Earth Sci. 5, 14. https://doi.org/10.3389/feart.2017.00014.

Cavalcante, R.B.L., Ferreira, D.B., da, S., Pontes, P.R.M., Tedeschi, R.G., da Costa, C.P.W., de Souza, E.B., 2020. Evaluation of extreme rainfall indices from CHIRPS precipitation estimates over the Brazilian Amazonia. Atmos. Res. 238, 104879 https://doi.org/10.1016/j.atmosres.2020.104879.

Chisanga, C.B., Phiri, E., Shepande, C., Sichingabula, H., 2015. Evaluating CERES-Maize model using planting dates and nitrogen fertilizer in Zambia. J. Agric. Sci. 7, p79. https://doi.org/10.5539/jas.v7n3p79.

Cover, T., Hart, P., 1967. Nearest neighbor pattern classification. IEEE Trans. Inf. Theory 13, 21–27. https://doi.org/10.1109/TIT.1967.1053964.

Dinku, T., Ceccato, P., Connor, S.J., 2011. Challenges of satellite rainfall estimation over mountainous and arid parts of east Africa. Int. J. Remote Sens. 32, 5965–5979. https://doi.org/10.1080/01431161.2010.499381.

Duncan, W.G., Loomis, R.S., Williams, W.A., Hanau, R., 1967. A model for simulating photosynthesis in plant communities. Hilgardia 38, 181–205. https://doi.org/10.3733/hilg.v38n04p181.

Fall, C.M.N., Lavaysse, C., Drame, M.S., Panthou, G., Gaye, A.T., 2021. Wet and dry spells in Senegal: comparison of detection based on satellite products, reanalysis, and in situ estimates. Nat. Hazards Earth Syst. Sci. 21, 1051–1069. https://doi.org/10.5194/nhess-21-1051-2021.

Funk, C.C., Peterson, P.J., Landsfeld, M.F., Pedreros, D.H., Verdin, J.P., Rowland, J.D., Romero, B.E., Husak, G.J., Michaelsen, J.C., Verdin, A.P., 2014. A quasi-global precipitation time series for drought monitoring. Data Ser. 12. https://doi.org/10.3133/ds832.

Funk, C., Peterson, P., Landsfeld, M., Pedreros, D., Verdin, J., Shukla, S., Husak, G., Rowland, J., Harrison, L., Hoell, A., Michaelsen, J., 2015. The climate hazards infrared precipitation with stations—a new environmental record for monitoring extremes. Sci. Data 2, 150066. https://doi.org/10.1038/sdata.2015.66.

Gao, Y.C., Liu, M.F., 2013. Evaluation of high-resolution satellite precipitation products using rain gauge observations over the Tibetan plateau. Hydrol. Earth Syst. Sci. 17, 837–849. https://doi.org/10.5194/hess-17-837-2013.

Guan, K., Sultan, B., Biasutti, M., Baron, C., Lobell, D.B., 2015. What aspects of future rainfall changes matter for crop yields in West Africa? Geophys. Res. Lett. 42, 8001–8010. https://doi.org/10.1002/2015GL063877.

Gumindoga, W., Rientjes, T.H.M., Haile, A.T., Makurira, H., Reggiani, P., 2019. Performance of bias-correction schemes for CMORPH rainfall estimates in the Zambezi River basin. Hydrol. Earth Syst. Sci. 23, 2915–2938. https://doi.org/10.5194/hess-23-2915-2019.

Guo, Y., Yu, H., Kong, D., Yan, F., Liu, D., Zhang, Y., 2015. Effects of gradual soil drought stress on the growth, biomass partitioning, and chlorophyll fluorescence of Prunus mongolica seedlings. Turk. J. Biol. 39, 532–539. https://doi.org/10.3906/biy-1412-20.

Habib, E., ElSaadani, M., Haile, A.T., 2012. Climatology-focused evaluation of CMORPH and TMPA satellite rainfall products over the Nile Basin. J. Appl. Meteorol. Climatol. 51, 2105–2121. https://doi.org/10.1175/JAMC-D-11-0252.1.

Haile, A.T., Habib, E., Elsaadani, M., Rientjes, T., 2012. Inter-comparison of satellite rainfall products for representing rainfall diurnal cycle over the Nile basin. Int. J. Appl. Earth Obs. Geoinf. 21, 230–240. https://doi.org/10.1016/j.jag.2012.08.012.

Herold, N., Alexander, L.V., Donat, M.G., Contractor, S., Becker, A., 2016. How much does it rain over land? Geophys. Res. Lett. 43, 341–348. https://doi.org/10.1002/2015GL066615.

Hobouchian, M.P., Salio, P., García Skabar, Y., Vila, D., Garreaud, R., 2017. Assessment of satellite precipitation estimates over the slopes of the subtropical Andes. Atmos. Res. 190, 43–54. https://doi.org/10.1016/j.atmosres.2017.02.006.

Hoogenboom, G., 1991. Simulation of ecophysiological processes of growth in several annual crops. Agric. Syst. 36, 244. https://doi.org/10.1016/0308-521X(91)90030-E.

Huffman, G.J., Bolvin, D.T., Nelkin, E.J., Wolff, D.B., Adler, R.F., Gu, G., Hong, Y., Bowman, K.P., Stocker, E.F., 2007. The TRMM Multisatellite Precipitation Analysis (TMPA): Quasi-Global, multiyear, combined-sensor precipitation estimates at fine scales. J. Hydrometeorol. 8, 38–55. https://doi.org/10.1175/JHM560.1.

International Soil Reference and Information Centre, 2004. Soil and Terrain Database for Kenya (KENSOTER), version 2.0 [WWW Document]. URL ⟨https://data.isric.org/geonetwork/srv/api/records/73e27136–9efe-49e4-af35-fd98b841d467⟩ (accessed 4.27.21).

Jayanthi, H., Husak, G.J., Funk, C., Magadzire, T., Chavula, A., Verdin, J.P., 2013. Modeling rain-fed maize vulnerability to droughts using the standardized precipitation index from satellite estimated rainfall—Southern Malawi case study. Int. J. Disaster Risk Reduct. 4, 71–81. https://doi.org/10.1016/j.ijdrr.2013.02.001.

Jobard, I., Chopin, F., Berges, J.C., Roca, R., 2011. An intercomparison of 10-day satellite precipitation products during West African monsoon. Int. J. Remote Sens. 32, 2353–2376. https://doi.org/10.1080/01431161003698286.

Joint Committee For Guides In Metrology, 2012. Vocabulaire international de métrologie. VIM3: Int. Vocab. Metrol. 3, 104.

Joyce, R.J., Janowiak, J.E., Arkin, P.A., Xie, P., 2004. CMORPH: a Method that produces global precipitation estimates from passive microwave and infrared data at high spatial and temporal resolution. J. Hydrometeorol. 5, 487–503. https://doi.org/10.1175/1525-7541(2004)005<0487:CAMTPG>2.0.CO;2.

Joyce, R.J., Xie, P., Yarosh, Y., Janowiak, J.E., Arkin, P.A., 2010. CMORPH: a "Morphing" approach for high resolution precipitation product generation. In: Gebremichael, M., Hossain, F. (Eds.), Satellite Rainfall Applications for Surface Hydrology. Springer Netherlands, Dordrecht, pp. 23–37. https://doi.org/10.1007/978-90-481-2915-7_2.

Li, Y., Guan, K., Schnitkey, G.D., DeLucia, E., Peng, B., 2019. Excessive rainfall leads to maize yield loss of a comparable magnitude to extreme drought in the United States. gcb.14628 Glob. Change Biol. 25, 2325–2337. https://doi.org/10.1111/gcb.14628.

Luetkemeier, R., Stein, L., Drees, L., Müller, H., Liehr, S., 2018. Uncertainty of rainfall products:iImpact on modelling household nutrition from rain-fed agriculture in Southern Africa. Water 10, 499. https://doi.org/10.3390/w10040499.

Maggioni, V., Vergara, H.J., Anagnostou, E.N., Gourley, J.J., Hong, Y., Stampoulis, D., 2013. Investigating the applicability of error correction ensembles of satellite rainfall products in river flow simulations. J. Hydrometeorol. 14, 1194–1211. https://doi.org/10.1175/JHM-D-12-074.1.

Masupha, T.E., Moeletsi, M.E., 2020. The use of Water Requirement Satisfaction Index for assessing agricultural drought on rain-fed maize, in the Luvuvhu River catchment, South Africa. Agric. Water Manag. 237, 106142 https://doi.org/10.1016/j.agwat.2020.106142.

McMillan, H., Jackson, B., Clark, M., Kavetski, D., Woods, R., 2011. Rainfall uncertainty in hydrological modelling: an evaluation of multiplicative error models. J. Hydrol. 400, 83–94. https://doi.org/10.1016/j.jhydrol.2011.01.026.

Mekonnen, K., Melesse, A.M., Woldesenbet, T.A., 2021. Spatial evaluation of satellite-retrieved extreme rainfall rates in the Upper Awash River Basin, Ethiopia. Atmos. Res. 249, 105297 https://doi.org/10.1016/j.atmosres.2020.105297.

Ndamani, F., Watanabe, T., 2015. Influences of rainfall on crop production and suggestions for adaptation. Int. J. Agric. Sci. 5, 367–374.

Osakabe, Y., Osakabe, K., Shinozaki, K., Tran, L.-S.P., 2014. Response of plants to water stress. Front. Plant Sci. 5, 86. https://doi.org/10.3389/fpls.2014.00086.

Ovando, G., Sayago, S., Bocco, M., 2018. Evaluating accuracy of DSSAT model for soybean yield estimation using satellite weather data. ISPRS J. Photogramm. Remote Sens. 138, 208–217. https://doi.org/10.1016/j.isprsjprs.2018.02.015.

Pan, M., Li, H., Wood, E., 2010. Assessing the skill of satellite-based precipitation estimates in hydrologic applications (n/a-n/a). Water Resour. Res. 46. https://doi.org/10.1029/2009WR008290.

Parent, C., Nicolas, C., Audrey, B., Crevècoeur, M., Dat, J.F., 2008. An overview of plant responses to soil waterlogging. Plant Stress 20–27.

Ramarohetra, J., Sultan, B., Baron, C., Gaiser, T., Gosset, M., 2013. How satellite rainfall estimate errors may impact rainfed cereal yield simulation in West Africa. Agric. For. Meteorol. 180, 118–131. https://doi.org/10.1016/j.agrformet.2013.05.010.

dos Reis, J., Rennó, C., Lopes, E., 2017. Validation of satellite rainfall products over a mountainous watershed in a Humid subtropical climate region of Brazil. Remote Sens. 9, 1240. https://doi.org/10.3390/rs9121240.

Reynolds, C.A., Yitayew, M., Slack, D.C., Hutchinson, C.F., Huete, A., Petersen, M.S., 2000. Estimating crop yields and production by integrating the FAO Crop Specific Water Balance model with real-time satellite data and ground-based ancillary data. Int. J. Remote Sens. 21, 3487–3508. https://doi.org/10.1080/014311600750037516.

Riha, S.J., Wilks, D.S., Simoens, P., 1996. Impact of temperature and precipitation variability on crop model predictions. Clim. Change 32, 293–311. https://doi.org/10.1007/BF00142466.

Sah, R.P., Chakraborty, M., Prasad, K., Pandit, M., Tudu, V.K., Chakravarty, M.K., Narayan, S.C., Rana, M., Moharana, D., 2020. Impact of water deficit stress in maize: phenology and yield components. Sci. Rep. 10, 2944. https://doi.org/10.1038/s41598-020-59689-7.

Savva, A.P., Frenken, K., 2002. Crop water requirement and irrigation scheduling. Irrig. Man. Modul. 4.

Senay, G.B., Verdin, J., 2002. Evaluating the performance of a crop water balance model in estimating regional crop production, in: Proceedings of Pecora Symposium 15/ Land Satellite Information IV/ ISPRS Commission I/FIEOS. Denver, United States of America, p. 8.

Sivakumar, M.V.K., 1988. Predicting rainy season potential from the onset of rains in Southern Sahelian and Sudanian climatic zones of West Africa. Agric. For. Meteorol. 42, 295–305. https://doi.org/10.1016/0168-1923(88)90039-1.

Smith, T.M., Arkin, P.A., Bates, J.J., Huffman, G.J., 2006. Estimating bias of satellite-based precipitation estimates. J. Hydrometeorol. 7, 841–856. https://doi.org/10.1175/JHM524.1.

Sultan, B., Defrance, D., Iizumi, T., 2019. Evidence of crop production losses in West Africa due to historical global warming in two crop models. Sci. Rep. 9, 12834. https://doi.org/10.1038/s41598-019-49167-0.

Sun, Q., Miao, C., Duan, Q., Ashouri, H., Sorooshian, S., Hsu, K., 2018. A review of global precipitation data sets: data sources, estimation, and intercomparisons. Rev. Geophys. 56, 79–107. https://doi.org/10.1002/2017RG000574.

Tadross, M., Suarez, P., Lotsch, A., Hachigonta, S., Mdoka, M., Unga-nai, L., Lucio, F., Kamdonyo, D., Muchinda, M., 2007. Changes in growing-season rainfall characteristics and downscaled scenarios of change over southern Africa: implications for growing maize, IPCC regional expert meeting on regional impacts, adaptation, vulnerability, and mitigation. Nadi, Fiji.

Tan, M., Tan, K., Chua, V., Chan, N., 2017. Evaluation of TRMM Product for monitoring drought in the Kelantan river basin, Malaysia. Water 9, 57. https://doi.org/10.3390/w9010057.

Tapiador, F.J., Turk, F.J., Petersen, W., Hou, A.Y., García-Ortega, E., Machado, L.A.T., Angelis, C.F., Salio, P., Kidd, C., Huffman, G.J., de Castro, M., 2012. Global precipitation measurement: Methods, datasets and applications. Atmos. Res. 104–105, 70–97. https://doi.org/10.1016/j.atmosres.2011.10.021.

Thaler, S., Brocca, L., Ciabatta, L., Eitzinger, J., Hahn, S., Wagner, W., 2018. Effects of different spatial precipitation input data on crop model outputs under a Central European Climate. Atmosphere 9, 290. https://doi.org/10.3390/atmos9080290.

Tittonell, P., Shepherd, K., Vanlauwe, B., Giller, K., 2008. Unravelling the effects of soil and crop management on maize productivity in smallholder agricultural systems of western Kenya—an application of classification and regression tree analysis. Agric. Ecosyst. Environ. 123, 137–150. https://doi.org/10.1016/j.agee.2007.05.005.

Tramblay, Y., Thiemig, V., Dezetter, A., Hanich, L., 2016. Evaluation of satellite-based rainfall products for hydrological modelling in Morocco. Hydrol. Sci. J. 61, 2509–2519. https://doi.org/10.1080/02626667.2016.1154149.

Watson, J., Challinor, A., 2013. The relative importance of rainfall, temperature and yield data for a regional-scale crop model. Agric. For. Meteorol. 170, 47–57. https://doi.org/10.1016/j.agrformet.2012.08.001.

Wilks, D.S., 2006. Statistical methods in the atmospheric sciences, Second ed, International Geophysics Series. Elsevier Academic Press Publications,.

Worqlul, A.W., Maathuis, B., Adem, A.A., Demissie, S.S., Langan, S., Steenhuis, T.S., 2014. Comparison of rainfall estimations by TRMM 3B42, MPEG and CFSR with ground-observed data for the Lake Tana basin in Ethiopia. Hydrol. Earth Syst. Sci. 18, 4871–4881. https://doi.org/10.5194/hess-18-4871-2014.

Xianghu, L., Zhang, Q., Xu, C.-Y., 2014. Assessing the performance of satellite-based precipitation products and its dependence on topography over Poyang Lake basin. Theor. Appl. Climatol. 115, 713–729. https://doi.org/10.1007/s00704-013-0917-x.

Xie, P., Arkin, P.A., 1996. Analyses of global monthly precipitation using gauge observations, satellite estimates, and numerical model predictions. J. Clim. 9, 840–858. https://doi.org/10.1175/1520-0442(1996)009<0840:AOGMPU>2.0.CO;2.

Xie, P., Joyce, R., Wu, S., Yoo, S.-H., Yarosh, Y., Sun, F., Lin, R., 2017. Reprocessed, bias-corrected CMORPH global high-resolution precipitation estimates from 1998. J. Hydrometeorol. 18, 1617–1641. https://doi.org/10.1175/JHM-D-16-0168.1.

Yadav, M.K., Singh, R.S., Patel, C., 2013. Rainfall characteristics analysis for rice based cropping system at Varanasi, Uttar Pradesh. J. Agric. Phys. 13, 186–192.

Yang, W.-C., Lin, K.-H., Wu, C.-W., Chang, Y.-J., Chang, Y.-S., 2020. Effects of Waterlogging with different water resources on plant growth and tolerance capacity of four Herbaceous flowers in a bioretention basin. Water 12, 1619. https://doi.org/10.3390/w12061619.

Yang, Y., Luo, Y., 2014. Evaluating the performance of remote sensing precipitation products CMORPH, PERSIANN, and TMPA, in the arid region of northwest China. Theor. Appl. Climatol. 118, 429–445. https://doi.org/10.1007/s00704-013-1072-0.